SCIENCE CHINA
Chemistry

• REVIEWS • Progress of Projects Supported by NSFC
• SPECIAL ISSUE • Chemical Methodology

January 2014 Vol.57 No.1: 58–69
doi: 10.1007/s11426-013-5018-2

Recent advances in fabrication of monolayer colloidal crystals and their inverse replicas

YE XiaoZhou & QI LiMin*

Beijing National Laboratory for Molecular Sciences; State Key Laboratory for Structural Chemistry of Unstable and Stable Species; College of Chemistry, Peking University, Beijing 100871, China

Received August 6, 2013; accepted August 19, 2013; published online November 4, 2013

Monolayer colloidal crystals (MCCs) are two-dimensional (2D) colloidal crystals consisting of a monolayer of monodisperse colloidal particles arrayed with a 2D periodic order. In recent years, MCCs have attracted intensive interest because they can act as 2D photonic crystals and be used as versatile templates for fabrication of various 2D nanostructure arrays. In this review, we provide an overview of the recent progress in the controllable fabrication of MCCs and their inverse replicas. First, some newly-developed methods for the self-assembly of MCCs based on different strategies including interfacial assembly and convective assembly are introduced. Second, some representative novel methods regarding the fabrication of various functional 2D inverse replicas of MCCs, such as 2D arrays of nanobowls, nanocaps, and hollow spheres, as well as 2D monolayer inverse opals (MIOs), are described. In addition, the potential applications of MCCs and their inverse replicas are discussed.

monolayer colloidal crystals, 2D inverse replica, nanosphere lithography, self-assembly, replication, fabrication method

1 Introduction

As periodically ordered arrays of monodisperse colloidal particles, colloidal crystals represent a new class of self-assembled materials, which have demonstrated potential applications in a wide variety of fields, such as photonic crystals, chemical and biological sensing, wetting, display, catalysis, energy storage and conversion, and templates for chemical synthesis and nanofabrication [1–4]. Generally, highly monodisperse colloidal micro- or nanoparticles can self-assemble into two periodic structures under appropriate conditions, namely, three-dimensional (3D) and two-dimensional (2D) colloidal crystals. 3D colloidal crystals have drawn extensive attention owing to their practical applications as colloidal photonic crystals [5] or as templates for fabricating inverse opals [6]. On the other hand, 2D colloidal crystals, which are monolayer arrays of colloidal particles or monolayer colloidal crystals (MCCs), have also attracted intensive interest because they can act as 2D photonic crystals and be used as versatile templates in surface pattering or for fabrication of 2D arrays of various nanostructures [7, 8].

A variety of feasible strategies, including drop-coating, dip-coating, spin-coating, electrophoretic deposition, and self-assembly at the gas/liquid interface, have been developed to self-assemble monodisperse colloidal particles into different kinds of monolayer colloidal crystals, such as hexagonal-close-packed (hcp) MCCs, non-close-packed (ncp) and patterned MCCs, and binary colloidal crystals (BCCs) [8]. MCCs have proven to be very effective and versatile templates toward 2D patterned nanostructures owing to their low cost, high throughput, high reproducibility and easy controllability over the chemical composition and structural parameters. Moreover, deliberate combination with sophisticated fabrication and assembly techniques allows more flexibility in tuning the structural parameters such as size, shape, orientation, periodicity, as well as de-

*Corresponding author (email: liminqi@pku.edu.cn)

sirable control of the chemical composition and materials properties of the templated nanostructures [7–12]. For example, significant advances have been achieved in the fabrication of periodic arrays of one-dimensional (1D) nanostructures using MCCs as templates [13, 14]. It is noteworthy that the controllable fabrication of inverse replicas of MCCs, such as 2D periodic arrays of nanobowls, nanocaps, and hollow spheres, as well as 2D monolayer inverse opals (MIOs), is attracting increasing interest in recent years. It has been demonstrated that both MCCs and their inverse replicas show great potential in some important applications including chemical and biosensing, solar cells, light-emitting diodes (LEDs), and optical devices.

In this review, we provide an overview of the recent progress in the controllable fabrication of MCCs and their inverse replicas. First, some novel methods developed recently for the self-assembly of MCCs are introduced. Then, we describe some representative novel methods regarding the fabrication of various functional 2D inverse replicas of MCCs. Next, the properties and emerging applications of MCCs and their 2D inverse replicas are discussed. Finally, summary and outlook on future developments are provided.

2 Self-assembly of monolayer colloidal crystals

Monodisperse colloidal spheres can be readily self-assembled into MCCs by a variety of methods [8]. Since Denkov *et al.* [15] firstly reported the mechanism of 2D crystallization on substrates, many self-assembly approaches have been reported for the optimized preparation of high-quality MCCs. Recently, some remarkable progress has been made in the controllable fabrication of large-area MCCs with high quality through interfacial assembly and convective assembly. Moreover, some new methods have been developed to achieve the controlled self-assembly of monolayer binary colloidal crystals and MCCs with tailored patterns.

2.1 Interfacial assembly

It is a facile and efficient method to assemble large-area MCCs through self-assembly at the gas-liquid interface because this method allows the formation of a monolayer exclusively without variation in the layer thickness. In the self-assembly at the gas-liquid interface, monodisperse colloidal particles, typically polystyrene (PS) spheres in an ethanol-water suspension, are spread onto a water surface and spontaneously form close packed MCCs at the interface through attractive interactions among the particles. Controlled aggregation, ordering and consolidation of the monolayer may be facilitated by the addition of a spreading agent such as dodecylsulfate to lower the surface tension. Spreading of the particles is a consequence of the Gibbs-Marangoni effect that describes the movement of a fluid due to a gradient in surface tension, resulting in mass transfer along the fluid-fluid interface away from the regions of low surface tension [5]. Systematic study revealed that the interfacial assembly of MCCs would be affected by a variety of factors, such as the solubility parameter of spreading solvents, particle concentration, zeta potential of the particles in the suspension, surface tension of the water phase, hardness of the particles, and addition of a salt in the suspension [16]. Moreover, for the fabrication of large-area MCCs with improved quality, it is essential to delicately control the process of adding the colloidal suspension onto the water surface to avoid possible sediment of colloidal spheres into the liquid phase.

As an improvement of the previous method for self-assembly at the gas-liquid solution, we developed a procedure by dropping colloidal suspension onto the top of a cleaned horizontal glass slide that was placed in the center of a water-contained Petri dish (Figure 1(a)), instead of dropping colloidal suspension on the water surface directly [17]. With this approach, the sediment of colloidal spheres into the water phase were successfully avoided and almost all the colloidal spheres could float on the water surface and form a uniform colorful MCC film up to more than 20 cm^2 in area (Figure 1(b)). A small volume of sodium dodecylsulfate (SDS) solution was then dropped onto the water surface to lower the surface tension, which packed the MCC film closely. The MCC film could be easily picked up with a piece of solid substrate. Figure 1(c) shows a typical scanning electron microscopy (SEM) image of a PS MCC film transferred on a zinc foil, confirming the formation of a high-quality hcp MCC film over a large area. This assembly method was subsequently employed for the self-assembly of anisotropic MCCs at the water-air interface using amphiphilic mushroom cap-shaped colloidal particles [18].

For the fast interfacial assembly of highly homogeneous MCCs with larger sizes, a needle tip flow method was designed by Asher and co-workers [19]. As shown in Figure 2(a), the tip of a sharpened injection needle was positioned just in contact with the water surface and the suspension was slowly and smoothly layered onto the top of the water

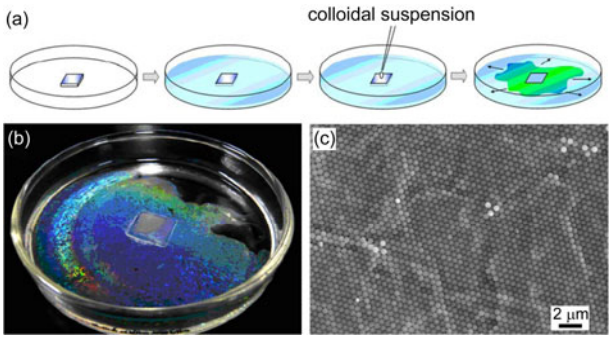

Figure 1 (a) Fabrication of a PS MCC by dropping colloidal suspension onto a solid substrate surrounded by water; (b) photograph of an MCC on the water surface in a glass dish ~ 6 cm in diameter; (c) SEM image of 450 nm PS MCC. Reprinted from Ref. [17].

surface to form monolayer arrays. The freshly formed particle arrays were radially pushed away from the needle tip to the outer edge of the dish and a beautiful continuous MCC film filled the entire water surface (> 280 cm^2) in 2 min (Figure 2(b)). It is essential that the contact of the needle tip with the water surface forms a meniscus structure along the needle tip wall, which damps the vertical flow forces to prevent breaking of the water surface to enable the layering of the colloid dispersion on the water surface. The floating 2D array can be transferred onto a substrate by either draining the water or by lifting the substrate. Both flat and curved substrates can be employed (Figure 2(c–e)). PS spheres ranging from 235 nm to 2 μm in size were successfully used for the fast fabrication of hcp MCCs at the air-water interface (Figure 2(f–i)).

Besides using water as liquid phase, Asher *et al*. [20] employed mercury as the liquid phase and the colloidal particle suspension spread rapidly on the interface because liquids with moderate surface suspension can spread readily on Hg as thin films. Although this method was very successful in preparing large-area MCCs, the use of Hg as a substrate is undesirable because of its toxicity. Recently, Wu *et al*. [21] reported a new method to assemble MCCs at water-oil interfaces. First, the hexane was added on the aqueous suspension of colloidal spheres to produce a water-oil interface. Then, an appropriate amount of ethanol was slowly added to the interface as an inducer and the colloidal spheres migrated to the interface. The colloidal spheres were compressed together to form ordered MCCs due to the surface pressure from the interfacial tension at the water-oil interface.

It may be noted that the interfacial assembly routes can be readily extended to the co-assembly of monolayer binary colloidal crystals. Some related work will be described in detail in Section 2.3.

2.2 Convective assembly

Convective assembly is another convenient technique for the fabrication of MCCs with large area and high quality. The basic principle is that colloidal nanospheres are transported from a reservoir into a meniscus that forms on a wetting substrate and are confined at the contact line. When the substrate is slowly withdrawn, the meniscus moves and the accumulated nanospheres are continuously deposited as a film, leading to the crystallization of MCCs [22]. As shown in Figure 3(a), there are three regions of convective particle assembly: In region I, the meniscus, free particles are convectively transported to the particle film. In region II, the particles are arranged to the particle film structure. In region III, the particles form a wet particle film with pronounced

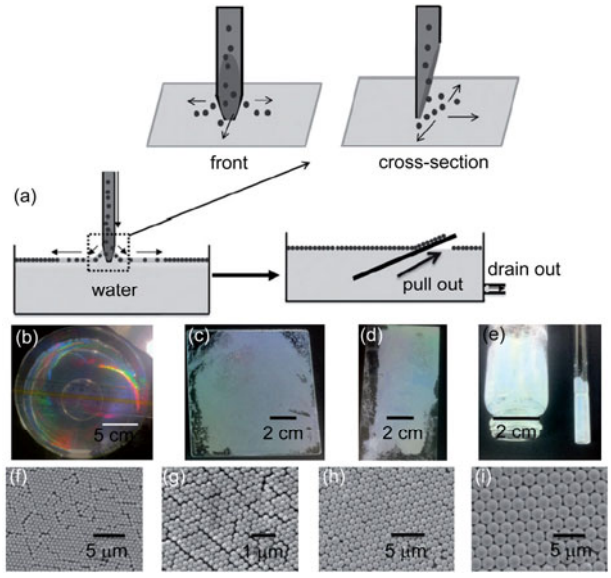

Figure 2 (a) Fabrication of a 2D PS particle array by the needle tip flow technique. The transfer of the 2D arrays onto a substrate is shown by draining out the water or by lifting the array on a substrate. (b) Photograph of 580 nm PS 2D array on the water surface in a glass dish 19 cm in diameter. 580 nm diameter PS 2D crystal arrays transferred onto (c) flat glass, (d) a plastic sheet, and (e) a curved glass. SEM images of 2D arrays of (f) 580 nm, (g) 235 nm, (h) 1 μm, and (i) 2 μm PS particles. Reprinted from Ref. [19].

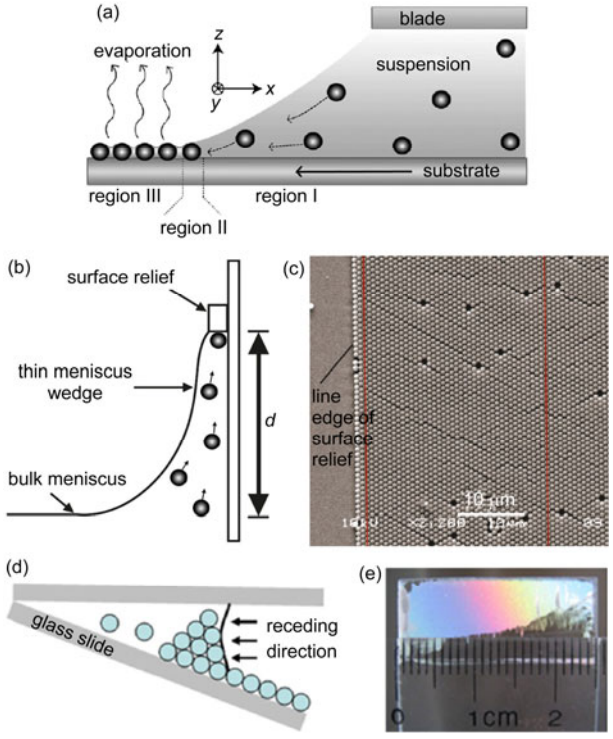

Figure 3 (a) Schematic illustration of convective particle assembly. Reprinted from Ref. [22]. (b) Illustration of pinned meniscus wedge at patterned surface relief. *d* is defined as the pinning distance as shown. (c) SEM image of domain-oriented growth of colloidal crystal from the edge of straight surface relief, producing high degree of directionality. Particles are lined up in the close-packed direction <10> or <11>, along the surface relief. Reprinted from Ref. [23]. (d) Schematic illustration of the gravity-assisted convective assembly process. (e) Photograph of a 2D colloidal crystal film formed by gravity-assisted convective assembly. Reprinted from Ref. [25].

evaporation. Crystallization of MCCs generally occurs in a transition region between the meniscus and the dried particle film.

Wong *et al*. [23] demonstrated the usage of meniscus pinning by surface relief boundaries to control in-plane orientation of monolayer colloidal crystals without interrupting grain orientation (Figure 3(b)). By optimizing the pinning boundary and withdrawal speed, a well controlled linear meniscus contact line offers unidirectional growth of a 2D colloidal crystal with the densely packed crystal direction <11> or <10> parallel to linear edge, giving rise to a single domain crystal with only twins and vacancies present as residual defects (Figure 3(c)). The pinning effect works by eliminating the wavy contact line induced by fingering instability which is commonly found in liquid wetting film. On the other hand, single-domain 2D colloidal crystals with centimeter size were fabricated in a wedge-shaped cell under capillary forces via the formation of a straight drying front [24]. Recently, this method was modified and centimeter-sized uniform MCCs were fabricated by gravity-assisted confined convective assembly [25]. The colloidal particles are transported to the edge of the suspension-glass interface mainly by gravity, and the transported particles are assembled into 2D colloidal crystal by the lateral capillary forces (Figure 3(d)). Using this method, uniform centimeter-sized MCCs can be formed under appropriate suspension concentration (Figure 3(e)), indicating an inexpensive, robust, and easily controlled method.

2.3 Self-assembly of monolayer binary colloidal crystals

Monolayer binary colloidal crystals (MBCCs) are monolayer colloidal crystals assembled by two kinds of monodisperse colloidal particles (usually with different sizes), which show rich arrays of crystal symmetries and different stoichiometries depending on the size ratio and particle concentration. In general, MBCCs can be assembled by two self-assembly strategies: stepwise assembly and co-assembly [8].

Recently, the formation of monolayer binary and ternary colloidal crystals through a simple and inexpensive confined-area evaporation-induced layer-by-layer (LBL) assembly method was reported [26]. In this stepwise assembly, large colloidal spheres were first assembled on substrates inside a rubber ring area due to the capillary forces caused by concave meniscus. Then, the formed MCCs were used as a template to localize the smaller particles, resulting in the growth of more complex types of crystals using the same confinement approach. Complex structures can form as a result of the interplay of the template layer effect, the surface forces exerted by the meniscus of the drying liquid, the space filling principle, and entropic forces. Meanwhile, the stepwise assembly of monolayer binary and ternary colloidal crystals was achieved by the preparation of hexagonal non-close-packed (hncp) MCCs through pyrolysis combined with plasma-electron coirradiation of hcp PS MCCs, which was followed by assembling small particles on the preformed hncp colloidal crystals [27].

There are also some recent reports on the facile co-assembly of monolayer binary colloidal crystals. Taking advantage of the self-assembly at the gas-liquid interface, Yan and co-workers [28] demonstrated an easy and fast process to fabricate large-area MBCCs with adjustable stoichiometries by co-self-assembly at the air-water interface with the assistance of the surfactant SDS. Recently, Cai *et al*. [29] presented a simple and facile approach to fabricate large-area MBCCs without any surfactants based on ethanol-assisted self-assembly at the water-air interface. The co-assembly of differently sized PS spheres was realized by injecting well-mixed suspensions of large and small PS spheres in mixed water-alcohol solution (1:1 in volume) along the edge of a water film preformed on a horizontally placed glass slide (Figure 4(a)). An MBCC was formed on the air-water interface after self-assembly and it was left on the slide after evaporation of liquid. The structure or pattern of the MBCCs could be designed from the established phase diagram and relatively accurately controlled by adjusting the volume ratios ($V_{S/L}$) of the small to large PS suspensions. For instance, a uniform BMCC with the pattern LS_9 pattern was prepared by the ethanol-assisted self-assembly route at $V_{S/L}$ = 0.048 (Figure 4(b, c)).

2.4 Other methods

In addition to the above mentioned approaches, some new

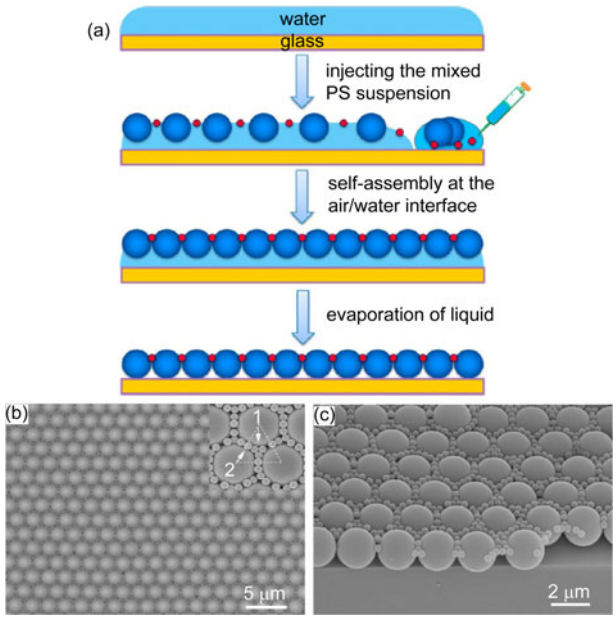

Figure 4 (a) Schematic illustration for the fabrication strategy of MBCCs based on ethanol-assisted self-assembly at the air-water interface. Top view (b) and side view (c) SEM images of monolayer binary colloidal crystals with a LS_9 pattern. Inset in (b) presents local magnified image showing LS_9 pattern. Reprinted from Ref. [29].

strategies or improved techniques have been reported for the preparation of MCCs with high quality and tunable patterns. For example, a novel attractive force gradient method was developed to fabricate high-quality, single-domain 2D colloidal crystals [30]. The attractive force gradient arises from a temperature gradient in the water-lutidine mixture. The nucleation of MCCs preferably occurs in the high-temperature region and crystallization propagates to the low-temperature region in a well-controlled way. Moreover, crack-free non-close-packed PS MCCs with a controllable inter-particle gap were obtained through convective assembly of colloidal PS spheres dispersed in tetraethylorthosilicate (TEOS) sol owing to the polymerization of TEOS sol during the self-assembly process [31]. In addition, face-centered cubic (fcc) (111)-orientated 2D and 3D crack-free silica colloidal crystals were fabricated on patterned silicon substrates via a vertical deposition method [32]. It was shown that monolayer of silica microspheres self-assembled on a hydrophobic substrate surface while multilayer of silica microspheres formed on a hydrophilic surface under otherwise the same experimental conditions.

3 Replication of monolayer colloidal crystals

MCCs can be employed as effective and versatile templates toward 2D patterned nanostructures such as 1D nanostructures arrays [13, 14], nanonets [33], and various 2D replicas of MCCs. Here we focus on the recent developments in the fabrication of periodic arrays of nanobowls, nanocaps, and hollow spheres as well as monolayer inverse opals (MIO) by replicating MCCs.

3.1 Nanobowl arrays

In principle, nanobowl arrays can be obtained if target materials are deposited only at the surfaces of the lower part of the colloidal nanospheres assembled into MCCs. Conventionally, nanobowl arrays on solid substrates are produced by assembling MCCs on the substrate followed by appropriate deposition processes including gas deposition and liquid deposition. For example, TiO_2 nanobowl arrays were prepared by a low-temperature atomic layer deposition (ALD) of TiO_2 on the preformed PS MCCs, which was followed by removal of the TiO_2 grown on the top-half of the PS spheres [34]. If a solution deposition is employed, the deposition process should be carefully controlled so that only the interstitial void spaces underneath the colloidal spheres are filled. Recently, Cai *et al*. [35] obtained WO_3 nanobowl arrays by calcination of the precursors, which were dropped and infiltrated into the interstices between substrates and MCCs. Huang *et al*. [36] successfully fabricated nanobowl arrays with several different materials including Ag, Pt, and MnO_2 through selective electrochemical deposition. In a similar way, polymer nanobowl arrays can be obtained through electropolymerization using MCCs as templates [37].

Recently, we have established a general approach towards free-standing, high-quality nanobowl arrays of various inorganic materials based on nanosphere lithography at solution surface (NSLSS), where MCCs floating at solution surface are employed as template for the deposition via reactions occurring near the gas-liquid interface [8]. The initial NSLSS process was induced by the diffusion of reactive gas into the aqueous solution containing the reactant metal ions (Figure 5(a)). For example, free-standing 2D ordered macroporous Ag thin films with a structure of nanobowl arrays can be readily produced by this method [38]. First, an hcp MCC was transferred onto the surface of $AgNO_3$ aqueous solution to form a floating MCC. Then, the gas-solution reaction between N_2H_4 and aqueous silver ions took place under the spatial confinement of the MCC template. When Ag^+ ions in the solution reduced to form Ag nanoparticles, the nucleation occurred preferentially at the gas-solution and solution-solid interfaces, hence the deposition of Ag occurred mostly at the lower surface of the spheres immersed in the $AgNO_3$ solution and at the triangular interstices among every three neighboring spheres. After adequate reaction and removal of MCC templates, free-standing Ag nanobowl arrays showing good mechanical robustness were formed (Figure 5(b, c)). Similarly, highly ordered nanobowl arrays of amorphous calcium carbonate (ACC) were obtained by NSLSS using the reaction between

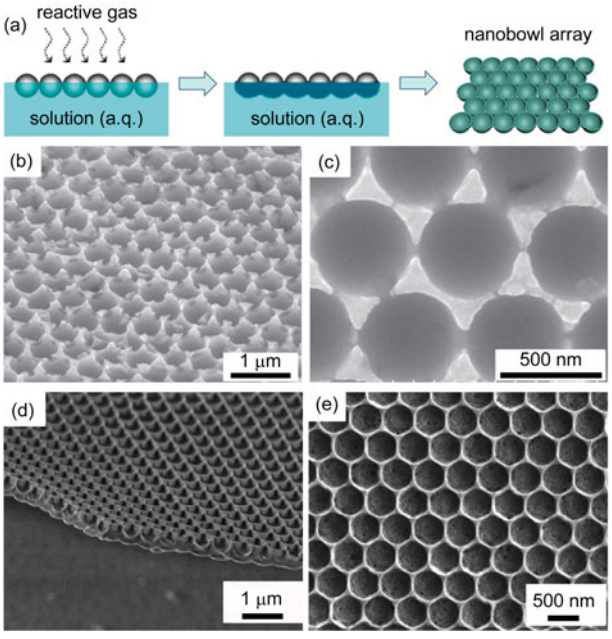

Figure 5 (a) Schematic illustration of the fabrication of inorganic nanobowl arrays by nanosphere lithography at solution surface through gas diffusion. SEM images of Ag nanobowl arrays produced using 450 nm PS spheres: (b) tilted view, (c) top view. Reprinted from Ref. [38]. SEM images of ACC nanobowl arrays produced using a 470 nm PS MCC: (d) tilted view, (e) top view. Reprinted from Ref. [39].

diffusing CO_2 and Ca^{2+} ions in solution (Figure 5(d, e)) [39]. Such honeycomb-patterned ACC thin films can be transformed into honeycomb-patterned, crystalline calcite films with different microstructures upon crystallization.

Although the NSLSS through gas diffusion has been successfully used in the fabrication of varied nanobowl arrays, it is difficult to directly use the NSLSS based on gas diffusion for the fabrication of regular nanobowl arrays of inorganic materials with a relatively high solubility. Therefore, a modified NSLSS through direct solution deposition (Figure 6(a)) was developed and employed for the facile fabrication of large-area ZnS nanobowl arrays with high regularity [40]. At first, hcp MCCs were transferred onto the surface of an aqueous reaction solution containing zinc acetate, thioacetamide (TAA), ammonium acetate, and disodium ethylenediamine tetraacetic acid (Na_2EDTA) to form floating MCCs. During the reaction at 60 ºC, S^{2-} ions were slowly released from TAA and reacted with Zn^{2+} ions in solution to form ZnS. The reaction preferentially occurred at the interface between negatively charged colloidal spheres and aqueous solution, leading to the formation of ZnS nanobowl arrays after removing the MCC template. Side views of the ZnS nanobowl arrays clearly show that the circular units are not net-like structures with through pores but bowl-like structures (Figure 6(b, c)). The top view shown in Figure 6(d) suggests that the nanobowl arrays had a uniform wall thickness of about 80 nm and a periodicity consistent with the diameter of PS spheres. The bottom-view shown in Figure 6(e) suggests that the nanobowls had closed bottom walls made of ZnS nanoparticles.

Interestingly, Fujii and co-workers [41] reported a facile method to make soft Janus-type 2D colloidal crystal films consisting of polypyrrole (PPy) coated PS microspheres using an air-water interface as a place to introduce softness, asymmetry, and regularity. The composite film had colloidal-crystal structure with particle monolayer thickness (Figure 7(a)). The air-exposed side of the film showed incomplete coverage of the PS particles with PPy, leaving a spherical cap of each particle uncoated (Figure 7(b)). PPy completely coated the PS spheres that had been facing the aqueous phase (Figure 7(c)). After removal of PS spheres with tetrahydrofuran, arrays of micrometer-sized PPy cups were produced (Figure 7(d)). This PPy cup array formed flexible films and the volume of a single PPy cup was calculated to be 7.6 fL, indicating the formation of a 2D femtoliter cup array, which could be useful for femtoliter-scale chemistry.

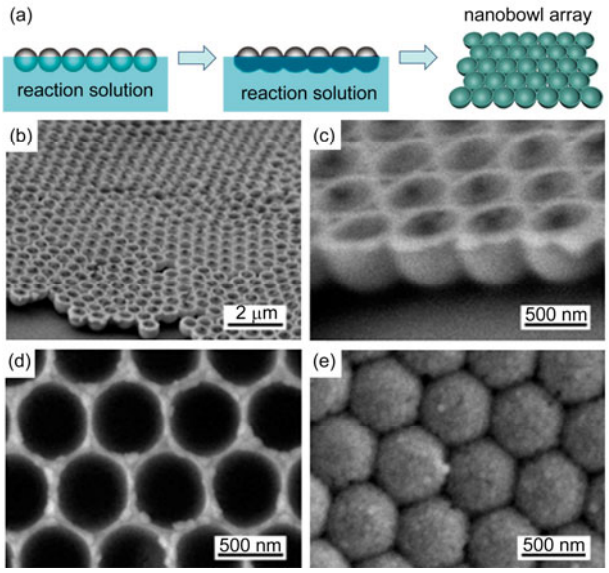

Figure 6 (a) Schematic illustration of the fabrication of inorganic nanobowl arrays by nanosphere lithography at solution surface through direct solution deposition. SEM images of ZnS nanobowl arrays produced using 600 nm PS spheres: (b, c) side view, (d) top view, (e) bottom view. Reprinted from Ref. [40].

3.2 Arrays of hollow spheres and nanocaps

Periodic arrays of hollow spheres can be obtained by deposition of desired materials around colloidal spheres, which are commonly achieved by electrochemical deposition. Normally, MCCs are coated on a conductive substrate that functions as work electrode. During the electrochemical deposition, the nucleation of target materials takes place at the substrate and the surface of colloidal spheres; hence hollow spheres are formed after the removal of MCC templates. The morphology of the as-prepared structures can be adjusted by varying the condition of electrochemical deposition. For example, Elias *et al*. [42] produced arrays of hollow urchin-like ZnO particles by making the nucleation take place on the PS spheres and the conductive substrate simultaneously (Figure 8(a)). The key point for the nucleation on the PS sphere surface is treating them with $ZnCl_2$ at

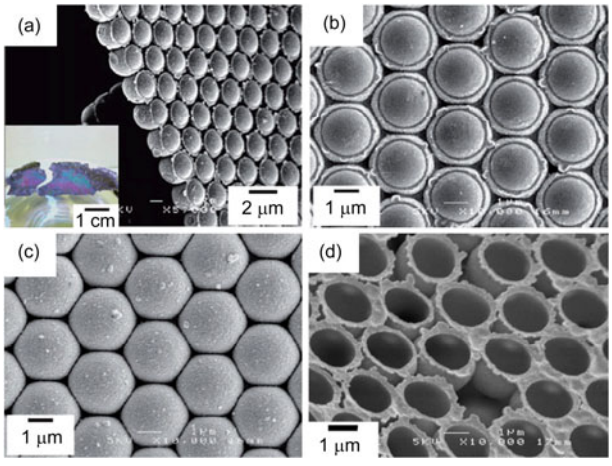

Figure 7 SEM images of a PPy-PS Janus colloidal crystal film produced at air-water interface using 2.5 μm PS spheres (a–c) and PPy femtoliter cup array after extraction of the PS spheres (d). Inset of (a) shows the Janus colloidal crystal films floating on the water surface under sunlight. SEM images were recorded from the air-exposed (b) and water-exposed (c) sides of the film. Reprinted from Ref. [41].

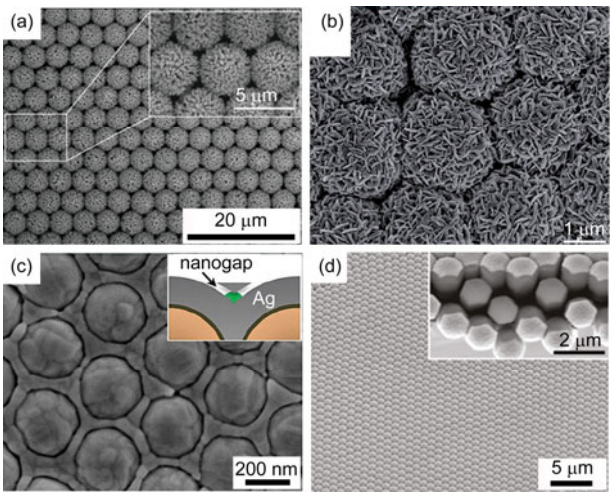

Figure 8 SEM images of 2D arrays of various hollow structures and caps. (a) Arrays of hollow urchin-like structure of ZnO nanowires. The inset is a magnified SEM image. Reprinted from Ref. [42]. (b) Arrays of hollow spheres made of standing Ag nanoplates. Reprinted from Ref. [43]. (c) Arrays of Ag nanoring cavities on the Ag film-over-nanosphere (AgFON) substrate. The inset is a schematic of the cross- sectional structure. Reprinted from Ref. [46]. (d) Arrays of Ag-a-Si metallo-dielectric (MD) multilayer nanocaps on PS spheres. The inset is a magnified SEM image. Reprinted from Ref. [47].

high concentration, which renders them electrically conductive. Recently, a simple and flexible strategy is presented to fabricate the Ag nanoplate-built hollow microsphere arrays based on electrodeposition onto the Au-coated MCC template [43]. The array consists of periodically arranged micro-sized hollow spheres, which are built by vertically standing and cross-linking Ag nanoplates several hundred nanometers in the planar dimension and about 30 nm in thickness (Figure 8(b)). In addition to electrochemical deposition, electrophoretic deposition can also be used to fabricate hollow sphere arrays via MCC template. For example, the electrophoretic deposition of charged Ag nanoparticles on the MCC-covered electrode resulted in the formation of Ag nanoshells on PS spheres [44].

On the other hand, gas deposition via evaporation/ sputtering is also a most commonly used method to fabricate periodic arrays of hollow spheres and caps with MCC templates. For instance, Au hollow sphere arrays can be easily fabricated by ion-sputtering Au on the ncp PS MCCs obtained by plasma etching [45]. Complicated and delicate structures may also be achieved through gas deposition. Oh *et al.* [46] reported a novel method for high-throughput fabrication of arrays of Ag nanoring cavities on Ag film-over-nanosphere (AgFON) substrate by combining MCC templates with atomic layer deposition (ALD) and ion milling. A typical SEM image of the Ag nanoring cavities on Ag-coated PS spheres with 10 nm gap is shown in Figure 8(c). If the sputtered materials only deposited on the upper half of the colloidal spheres of MCC templates, nanocap arrays could be fabricated. As an example, novel metallo-dielectric (MD) multilayer nanocap arrays consisting of alternating layers of Ag and amorphous Si (a-Si) were achieved on MCC templates by finely controlling fabrication condition (Figure 8(d)) [47]. Notably, hexagonal-patterned monolayer arrays of TiO_2 hollow hemispheres and spheres with thin shells of ~10 nm were fabricated using PS MCCs as templates by sputtering and wet coating approaches, respectively [48]. Owing to their precisely adjustable structural parameters, the prepared hollow hemisphere/ sphere films exhibited widely tunable visible-light reflection and absorption bands.

3.3 Monolayer inverse opals

Recently, considerable attention has been paid to the controllable fabrication of functional monolayer inverse opals (MIOs) by replicating MCCs. For example, Park *et al*. [49] reported a procedure for the fabrication of 2D TiO_2 inverse opals using PS MCC template (Figure 9(a)). The MCC template was covered with TiO_x sol solution by a doctor blade technique, where the deposition thickness is critical factor for fabrication of the 2D TiO_2 inverse opal with a closed top surface. After the solvent was evaporated, calcination was performed, not only to remove the MCC templates,

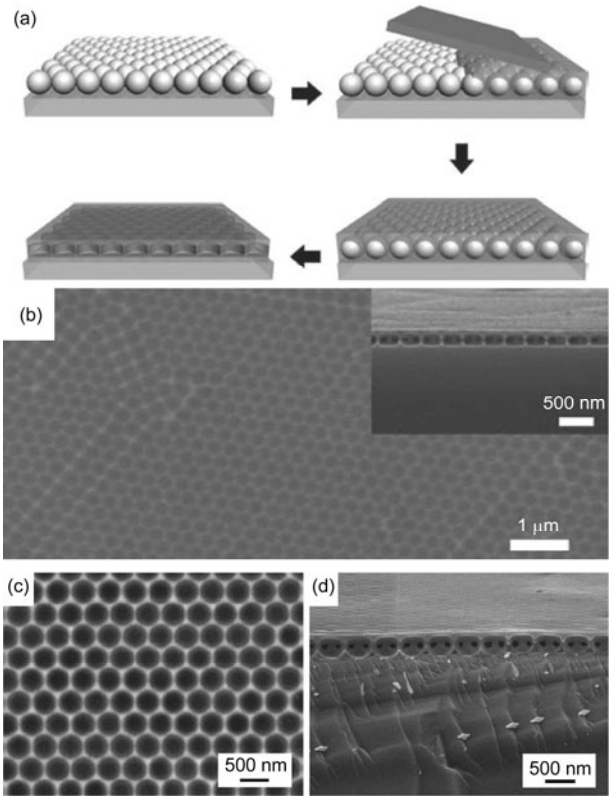

Figure 9 (a) Schematic illustration for the fabrication of 2D TiO_2 inverse opal with closed top-surface. (b) SEM images of top and cross-sectional (inset) views of 2D TiO_2 inverse opal. Reprinted from Ref. [49]. SEM images of top (c) and cross- sectional (d) views monolayer inverse opal of polyelectrolyte gel on a silicon wafer. Reprinted from Ref. [50].

but also to transform the amorphous phase of TiO_2 into a crystalline phase, leading to an increase of the refractive index and mechanical property. A representative SEM image of the fabricated 2D TiO_2 inverse opal with a closed top-surface structure is shown in Figure 9(b). The insert shows its cross-sectional view, which indicates that the voids look elliptical or almost rectangular. Apart from MIOs made of inorganic materials like TiO_2, stimuli-responsive polyelectrolyte MIOs were also obtained by a similar procedure using MCCs as template [50]. The SEM images of the polyelectrolyte MIOs show that the polyelectrolyte gel replicated well the hexagonal order of the MCC template (Figure 9(c, d)).

4 Applications of MCCs and their inverse replicas

MCCs and their inverse replicas have demonstrated potential applications in a variety of important areas including chemical and biosensing, solar cells, LEDs, and optical devices. Particularly, there is significant interest in applying them as chemical and biosensors based on the photonic bandgap properties and surface-enhanced Raman scattering (SERS) properties. Here we just present several representative examples with emphasis on the sensing applications based on 2D photonic crystals and SERS.

Novel 2D photonic crystal sensors based on MCCs [20] or MIOs [50] were successfully fabricated by employing stimuli-responsive polymer hydrogel thin films and used for Pb^{2+} ion and pH sensing. It has been demonstrated that such 2D photonic crystal sensors have multiple advantages over the traditional 3D photonic crystal sensors, such as fast detection of small volumes as well as ease of fabrication and functionalization. If MCCs were embedded in a poly(*N*-isopropylacrylamide) (PNIPAAm)-based hydrogel film, the resultant 2D photonic crystal sensor can be employed for visual determination of surfactant molecules [51]. It is noteworthy that novel 2D biotin hydrogel sensors, which were fabricated by attaching MCCs onto the surface of hydrogels containing biotin, can be used for visual determination of avidin molecules via protein recognition [52]. Figure 10(a) shows the diffraction spectra of the 2D biotin hydrogel sensors in different concentrations of avidin in 0.1 M NaCl. The diffraction wavelength blue shifts with increasing avidin concentrations. Figure 10(b) shows that the diffraction shifts from red to yellow, and then to green with increasing avidin concentrations. The blue shift is caused by the strong avidin–biotin binding crosslinks formed in the hydrogel sensors, which shrink the hydrogel and decrease the 2D array spacing (Figure 10(c)).

The sensing process of the 2D photonic crystal sensors made of polymer hydrogels is generally based on the volume changes in aqueous solution, which may still suffer from relatively slow response time and limited working environments. Hence it is worthwhile to explore the fabrication of sensitive 2D photonic crystal sensors made of rigid materials. In this regard, the ZnS nanobowl arrays shown in Figure 6 have proved to be effective, fast-responsive 2D photonic crystal sensors for oil sensing based on the refractive index changes [40].The transmission spectra of the ZnS nanobowl arrays immersed in various solvents were recorded and the two typical spectra in ethanol and toluene together with that in air are presented in Figure 11(a). The variation of the band gap shifts versus the refractive index of solvents exhibits a good linear relationship in the refractive

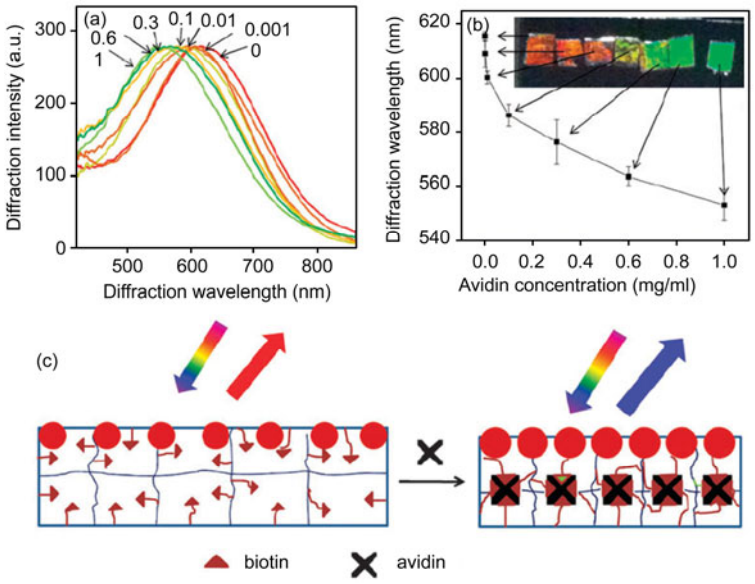

Figure 10 (a) Dependence of normalized diffraction spectra of 2D biotin hydrogel sensors upon avidin concentration. (b) Dependence of diffraction wavelength on avidin concentration. Inset shows the related photographs (c) Schematic showing the binding of avidin molecules to multiple hydrogel biotins, which increases the crosslinking, blue shifting the diffraction. Reprinted from Ref. [52].

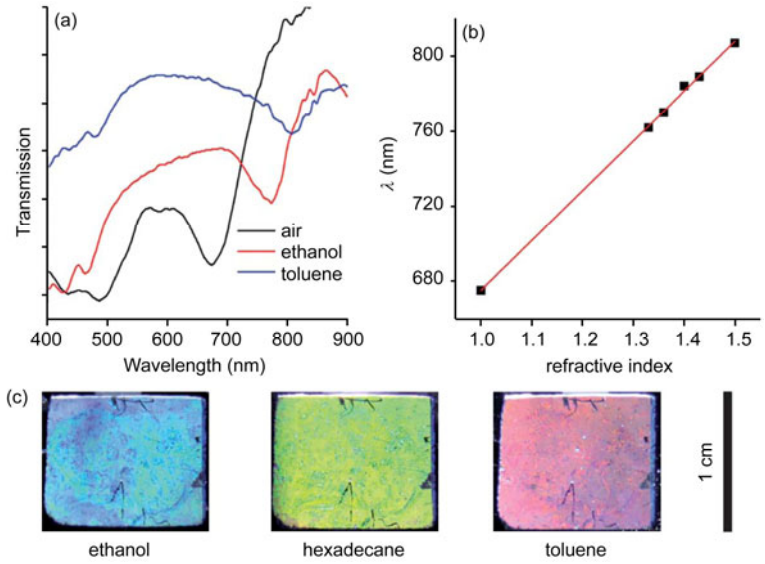

Figure 11 (a) Transmission spectra of ZnS nanobowl arrays immersed in different organic solvents; (b) relationship between the stop band position and the refractive index of solvents; (c) optical photographs of ZnS nanobowl arrays immersed in three different solvents. Reprinted from Ref. [40].

index range from 1 to 1.50 (Figure 11(b)), which covers the refractive index range for most organic solvents. Notably, the procedure for oil sensing is very simple and the responsive time is very short (less than 1 second), which would be advantageous in detecting viscous oils and in terms of processing. The ZnS nanobowl arrays could also visualize refractive index change by color changes (Figure 11(c)). Furthermore, After surface functionalization, the ZnS nanobowl arrays can be used as effective 2D photonic crystal biosensors for sensitive detection of avidin molecules with low detection limits (less than 100 pM) and broad working range.

SERS is a powerful technique for sensitive and selective detection, which rests in the use of roughened, coinage metal surfaces to amplify scattering. Recently, the low-cost fabrication of more precisely defined metal MCC replicas is pursued because these structures may provide more reliable performance while still leading to reasonably large SERS enhancement factors. Fang *et al*. fabricated Ag film on nanospheres as SERS substrates and measured the distribution of site enhancements [53]. They demonstrated the existence of ''hot spots'' and the great contribution to the whole SERS signal from a few amount molecules at hot spots. Moreover, Farcau and Astilean confirmed the site of hot spots on Au film-on-nanospheres through mapping and demonstrated that the mostly enhanced electromagnetic (EM) field is confined at the edges and sharp crevices between adjacent metallic half-shells [54].

In recent years, different kinds of novel structures have been designed and fabricated to enhance SERS performances of the inverse replicas of MCCs. For example, Lee *et al*. reported Ag-a-Si metallo-dielectric photonic crystals (MDPC) that can be used as ultrasensitive molecular detectors for concentrations down to picomolar level based on SERS [47]. The structure information of Ag-a-Si MDPC is schematically summarized in Figure 12(a) and the morphology is shown in Figure 8(d). For the detection of R6G with concentration of 10^{-12} M, the MDPCs with multiple MD units show stronger Raman signals than the reference one, and the MDPC with 4 MD units shows the strongest intensity (Figure 12(b)). Recently, Oh *et al*. [46] demonstrated a hybrid SERS substrate (FON-gap) that combined the tunable localized surface plasmon resonance (LSPR) of AgFON substrates with a strong field enhancement inside 10-nm metallic nanogaps. The structure information of the AgFON and FON-gap is schematically shown in Figure 12(c) and the morphology can be seen in Figure 8(c). In Figure 12(d), both a FON-10 nm gap and AgFON substrates were exposed to decreasing concentrations of adenine, and the intensity of the purine stretch at 731 cm^{-1} shift was used to evaluate limits of detection. The adenine signal on the FON-gap substrate was more intense than that observed on the AgFON and can be attributed to the adenine molecules experiencing higher electromagnetic fields at the surface of the FON-gap compared to those on the AgFON surface. The average enhancement factor of near 10^8 for the FON-gap substrates is not only higher than previously reported large-area SERS substrates, but also improving the robust AgFON substrate toward the theoretical maximum enhancement factor of 10^9, demonstrating that the FON-gap substrates can be used to detect lower levels of analyte compared to traditional sensing platforms.

Besides the sensing applications, the 2D replicates of MCCs as well as the 2D composites with MCCs have shown other promising applications. Up to now, some energy-related materials with specifically designed structures have been fabricated with the assistance of MCCs, aiming at improving light harvesting efficiency. For instance, quasi-

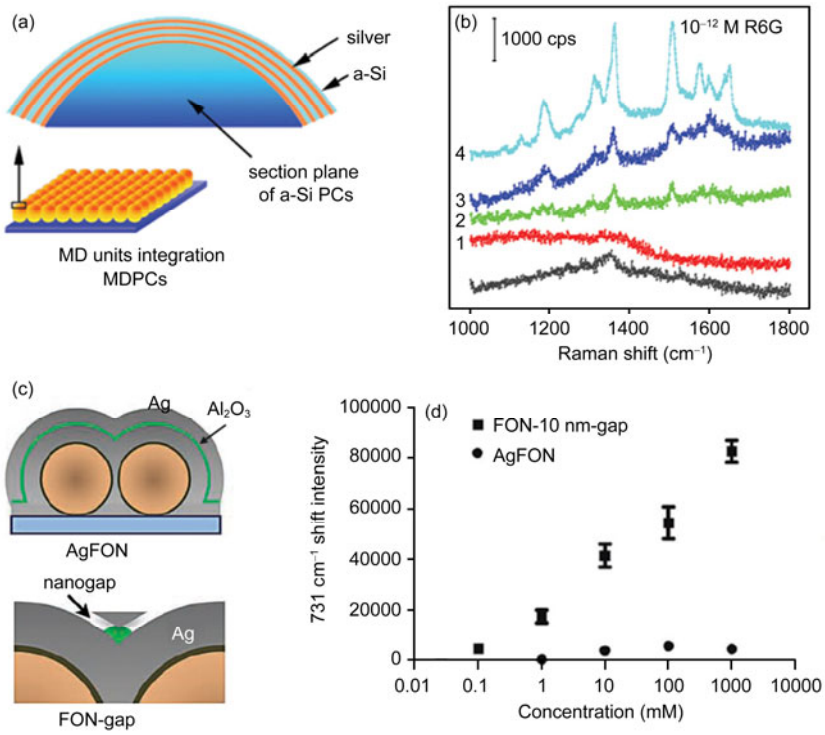

Figure 12 (a) Schematic illustration of the structure of Ag-a-Si metallo-dielectric photonic crystals (MDPCs). (b) Raman spectra recorded from MDPCs with a R6G concentration of 10–12 M. The colored curves are obtained from MDPCs with different MD units with the MD unit number labeled from 1 to 4. The dark gray curves are obtained from the reference substrate. Reprinted from Ref. [47]. (c) Schematic cross-sections of AgFON and FON-gap. (d) A limit of detection plot for SERS Biosensing where the intensity of the purine stretch of adenine is plotted versus adenine concentration. Reprinted from Ref. [46].

ordered TiO_2 hollow hemispheres prepared with the assistance of MCCs were demonstrated to be useful for dye-sensitized solar cells [55]. Thanks to the hollow structure that could promote electron transport and the large surface area that would allow the enhancement of dye loading, the as-prepared hollow TiO_2 hemisphere arrays exhibited an enhanced photo-conversion efficiency. Moreover, Park *et al.* [49] demonstrated experimentally and numerically the enhanced light extraction efficiency of a polymer LED by inserting a 2D TiO_2 inverse opal structure, which is shown in Figure 9(b), between the glass and anode electrode. The principle of the enhanced light extraction of LED with the 2D TiO_2 inverse opal is that the 2D inverse opal suppresses the waveguided loss by creating a photonic bandgap of diffracting the waveguided light. In addition, the hybrid colloidal plasmonic-photonic crystals consisting of MCCs and metal coatings represent a new platform that may lead to the realization of different optical functions [56, 57].

5 Summary and outlook

In this review, we have summarized some recent advances in the self-assembly and replication of MCCs, as well as the potential applications of MCCs and their 2D inverse replica. The facile and controllable fabrication of large-area and high-quality MCCs has been a long-pursued goal. Remarkable progress has been made toward this goal in recent years through different self-assembly strategies, especially the interfacial assembly and the convective assembly. Moreover, some new methods or improved techniques have been developed for the preparation of MCCs and MBCCs with high quality and tunable patterns. The nanosphere lithography or MCC-based colloidal lithography, which employs self-assembled 2D colloidal crystals as templates for the controlled deposition of target materials, has been demonstrated to be a facile, low-cost, and efficient route toward fabricating various 2D inverse replicas of MCCs. Typical examples are 2D periodic arrays of nanobowls, nanocaps and hollow spheres, as well as monolayer inverse opals. Deliberate combination between MCC templates with adjustable structural parameters and sophisticated fabrication and assembly techniques results in a great flexibility in tuning the structural parameters and properties of the final replicated nanostructures. Additionally, the MCCs and their 2D inverse replicas have shown promising potential applications in many important areas, such as chemical and biosensing, solar cells, LEDs, and optical devices.

Despite the exciting developments in the controllable fabrication of MCCs and their inverse replicas, many challenges still remain ahead. Firstly, the facile and reproducible fabrication of defect-free MCCs in a large area is still a goal to pursue. Meanwhile, the controllable assembly of MCCs with more complex patterns such as MCCs made of non-

spherical particles or multiple components remains a challenge. In this regard, the strategies employed for the self-assembly of inorganic nanoparticles into 2D superstructures [58–60] may provide some inspiration for the fabrication of unique 2D colloidal crystals. Secondly, it is desirable to explore much simpler, more controllable and flexible approaches toward the fabrication of 2D inverse replicas of MCCs. It is also demanding to realize the preparation of the 2D inverse replicas with even more complex patterns and with desirable chemical components. Finally, although many potential applications of MCCs and their inverse replicas have been demonstrated, great efforts are still needed to investigate the relationship between the application performance and the structural parameters, to further improve the properties and performance, and to achieve their practical applications in many technologically important fields.

This work was supported by the National Natural Science Foundation of China (21173010, 21073005, and 51121091) and Ministry of Science and Technology of China (2013CB932601).

1 Marlow F, Muldarisnur, Sharifi P, Brinkmann R, Mendive C. Opals: Status and prospects. *Angew Chem Int Ed*, 2009, 48: 6212–6233
2 Moon JH, Yang S. Chemical aspects of three-dimensional photonic crystals. *Chem Rev*, 2010, 110: 547–574
3 Li F, Josephson DP, Stein A. Colloidal assembly: The road from particles to colloidal molecules and crystals. *Angew Chem Int Ed*, 2011, 50: 360–388
4 Ge J, Yin Y. Responsive photonic crystals. *Angew Chem Int Ed*, 2011, 50: 1492–1522
5 von Freymann G, Kitaev V, Lotsch BV, Ozin GA. Bottom-up assembly of photonic crystals. *Chem Soc Rev*, 2013, 42: 2528–2554
6 Stein A, Wilson BE, Rudisill SG. Design and functionality of colloidal-crystal-templated materials—Chemical applications of inverse opals. *Chem Soc Rev*, 2013, 42: 2763–2803
7 Zhang J, Li Y, Zhang X, Yang B. Colloidal self-assembly meets nanofabrication: From two-dimensional colloidal crystals to nanostructure arrays. *Adv Mater*, 2010, 22: 4249–4269
8 Ye X, Qi L. Two-dimensionally patterned nanostructures based on monolayer colloidal crystals: Controllable fabrication, assembly, and applications. *Nano Today*, 2011, 6: 608–631
9 Yang SM, Jang SG, Choi DG, Kim S, Yu HK. Nanomachining by Colloidal Lithography. *Small*, 2006, 2: 458–475
10 Zhang G, Wang D. Colloidal lithography—The art of nanochemical patterning. *Chem-Asian J*, 2009, 4: 236–245
11 Yang S, Lei Y. Recent progress on surface pattern fabrications based on monolayer colloidal crystal templates and related applications. *Nanoscale*, 2011, 3: 2768–2782
12 Li Y, Duan G, Liu G, Cai W. Physical processes-aided periodic micro/nanostructured arrays by colloidal template technique: Fabrication and applications. *Chem Soc Rev*, 2013, 42: 3614–3627
13 Li L, Zhai T, Zeng H, Fang X, Bando Y, Golberg D. Polystyrene sphere-assisted one-dimensional nanostructure arrays: Synthesis and applications. *J Mater Chem*, 2011, 21: 40–56
14 Li Y, Koshizaki N, Cai W. Periodic one-dimensional nanostructured arrays based on colloidal templates, applications, and devices. *Coord Chem Rev*, 2011, 255: 357–373
15 Denkov ND, Velev OD, Kralchevsky PA, Ivanov IB, Yoshimura H, Nagayama K. Two-dimensional crystallization. *Nature*, 1993, 361: 26–26
16 Moon GD, Lee TI, Kim B, Chae G, Kim J, Kim S, Myoung JM, Jeong U. Assembled monolayers of hydrophilic particles on water surfaces. *ACS Nano,* 2011, 5: 8600–8612
17 Li C, Hong GS, Wang PW, Yu DP, Qi LM. Wet chemical approaches to patterned arrays of well-aligned ZnO nanopillars assisted by monolayer colloidal crystals. *Chem Mater*, 2009, 21: 891–897
18 Xu LA, Li H, Jiang X, Wang JX, Li L, Song YL, Jiang L. Synthesis of amphiphilic mushroom cap-shaped colloidal particles towards fabrication of anisotropic colloidal crystals. *Macromol Rapid Commun*, 2010, 31: 1422–1426
19 Zhang J-T, Wang L, Lamont DN, Velankar SS, Asher SA. Fabrication of large-area two-dimensional colloidal crystals. *Angew Chem Int Ed*, 2012, 51: 6117–6120
20 Zhang J-T, Wang L, Luo J, Tikhonov A, Kornienko N, Asher SA. 2-D array photonic crystal sensing motif. *J Am Chem Soc*, 2011, 133: 9152–9155
21 Chen H, Hu L, Fang X, Wu L. General fabrication of monolayer SnO_2 nanonets for high-performance ultraviolet photodetectors. *Adv Funct Mater*, 2012, 22: 1229–1235
22 Born P, Munoz A, Cavelius C, Kraus T. Crystallization mechanisms in convective particle assembly. *Langmuir*, 2012, 28: 8300–8308
23 Ng ECH, Chin KM, Wong CC. Controlling inplane orientation of a monolayer colloidal crystal by meniscus pinning. *Langmuir*, 2011, 27: 2244–2249
24 Sun J, Tang CJ, Zhan P, Han, ZL, Cao ZS, Wang ZL. Fabrication of centimeter-sized single-domain two-dimensional colloidal crystals in a wedge-shaped cell under capillary forces. *Langmuir*, 2010, 26: 7859–7864
25 Ye R, Ye Y-H, Zhou Z, Xu H. Gravity-assisted convective assembly of centimeter-sized uniform two-dimensional colloidal crystals. *Langmuir*, 2013, 29: 1796–1801
26 Singh G, Pillai S, Arpanaei A, Kingshott P. Layer-by-layer growth of multicomponent colloidal crystals over large areas. *Adv Funct Mater*, 2011, 21: 2556–2563
27 Kim JJ, Li Y, Lee EJ, Cho SO. Fabrication of size-controllable hexagonal non-close-packed colloidal crystals and binary colloidal crystals by pyrolysis combined with plasma-electron coirradiation of polystyrene colloidal monolayer. *Langmuir*, 2011, 27: 2334–2339
28 Yu J, Yan Q, Shen D. Co-self-assembly of binary colloidal crystals at the air-water interface. *ACS Appl Mater Interfaces*, 2010, 2: 1922–1926
29 Dai Z, Li Y, Duan G, Jia L, Cai W. Phase diagram, design of monolayer binary colloidal crystals, and their fabrication based on ethanol-assisted self-assembly at the air/water interface. *ACS Nano*, 2012, 6: 6706–6716
30 Sun X, Li Y, Zhang TH, Ma YQ, Zhang Z. Fabrication of large two-dimensional colloidal crystals via self-assembly in an attractive force gradient. *Langmuir*, 2013, 29: 7216–7220
31 Cai Z, Liu YJ, Leong ESP, Teng J, Lu X. Highly ordered and gap controllable two-dimensional non-close-packed colloidal crystals and plasmonic-photonic crystals with enhanced optical transmission. *J Mater Chem*, 2012, 22: 24668–24675
32 Cai Z, Teng J, Xia D, Zhao XS. Self-assembly of crack-free silica colloidal crystals on patterned silicon substrates. *J Phys Chem C*, 2011, 115: 9970–9976
33 Li C, Hong G, Qi L. Nanosphere lithography at the gas/liquid interface: A general approach toward free-standing high-quality nanonets. *Chem Mater* 2010, 22: 476–481
34 Wang X, Lao C, Graugnard E, Summers CJ, Wang ZL. Large-size liftable inverted-nanobowl sheets as reusable masks for nanolithiography. *Nano Lett*, 2005, 5: 1784–1788
35 Zhang H, Duan G, Liu G. Li Y, Xu X, Dai Z, Wang J, Cai W. Layer-controlled synthesis of WO_3 ordered nanoporous films for optimum electrochromic application. *Nanoscale*, 2013, 5: 2460–2468

36 Yang S, Lapsley MI, Cao B, Zhao C, Zhao Y, Hao Q, Kiraly B, Scott J, Li W, Wang L, Lei Y, Huang TJ. Large-scale fabrication of three-dimensional surface patterns using template-defined electrochemical deposition. *Adv Funct Mater*, 2013, 23: 720–730

37 Pernites RB, Foster EL, Felipe MJL, Robinson M, Advincula RC. Patterned surfaces combining polymer brushes and conducting polymer via colloidal template electropolymerization. *Adv Mater*, 2011, 23: 1287–1292

38 Hong G, Li C, Qi LM. Facile fabrication of two-dimensionally ordered macroporous silver thin films and their application in molecular sensing. *Adv Funct Mater*, 2010, 20: 3774–3783

39 Li C, Hong G, Yu H, Qi L. Facile fabrication of honeycomb-patterned thin films of amorphous calcium carbonate and mosaic calcite. *Chem Mater*, 2010, 22: 3206–3211

40 Ye X, Li Y, Dong J, Xiao J, Ma Y, Qi L. Facile synthesis of ZnS nanobowl arrays and their applications as 2D photonic crystal sensors. *J Mater Chem C*, 2013, 1: 6112–6119

41 Fujii S, Kappl M, Butt H-J, Sugimoto T, Nakamura Y. Soft Janus colloidal crystal film. *Angew Chem Int Ed*, 2012, 51: 9809–9813

42 Elias J, Levy-Clement C, Bechelany M, Michler J, Wang GY, Wang Z, Philippe L. Hollow urchin-like ZnO thin films by electrochemical deposition. *Adv Mater*, 2010, 22: 1607–1612

43 Liu G, Cai W, Kong L, Duan G, Li Y, Wang J, Zuo G, Cheng Z. Standing Ag nanoplate-built hollow microsphere arrays: Controllable structural parameters and strong SERS performances. *J Mater Chem*, 2012, 22: 3177–3184

44 Yang S, Cai W, Kong L, Lei Y. Surface nanometer-scale patterning in realizing large-scale ordered arrays of metallic nanoshells with well-defined structures and controllable properties. *Adv Funct Mater*, 2010, 20: 2527–2533

45 Liu G, Li Y, Duan G, Wang J, Liang C, Cai W. Tunable surface plasmon resonance and strong SERS performances of Au opening-nanoshell ordered arrays. *ACS Appl Mater Interfaces*, 2012, 4: 1–5

46 Im H, Bantz KC, Lee SH, Johnson TW, Haynes CL, Oh SH. Self-assembled plasmonic nanoring cavity arrays for SERS and LSPR biosensing. *Adv Mater*, 2013, 25: 2678–2685

47 Zhao Y, Zhang XJ, Ye J, Chen LM, Lau SP, Zhang WJ, Lee ST. Metallo-dielectric photonic crystals for surface-enhanced Raman scattering. *ACS Nano*, 2011, 5: 3027–3033

48 Li J, Qin Y, Jin C, Li Y, Shi D, Schmidt-Mende L, Gan L, Yang J. Highly ordered monolayer/bilayer TiO_2 hollow sphere films with widely tunable visible-light reflection and absorption bands. *Nanoscale*, 2013, 5: 5009–5016

49 Hyun WJ, Lee HK, Oh SS, Hess O, Choi C-G, Im SH, Park OO. Two-dimensional TiO_2 inverse opal with a closed top surface structure for enhanced light extraction from polymer light-emitting diodes. *Adv Mater*, 2011, 23: 1846–1850

50 Li C, Lotsch BV. Stimuli-responsive 2D polyelectrolyte photonic crystals for optically encoded pH sensing. *Chem Commun*, 2012, 48: 6169–6171

51 Zhang J-T, Smith N, Asher SA. Two-dimensional photonic crystal surfactant detection. *Anal Chem*, 2012, 84: 6416–6420

52 Zhang J-T, Chao X, Liu X, Asher SA. Two-dimensional array Debye ring diffraction protein recognition sensing. *Chem Commun*, 2013, 49: 6337–6339

53 Fang Y, Seong NH, Dlott DD. Measurement of the distribution of site enhancements in surface-enhanced Raman scattering. *Science*, 2008, 321: 388–392

54 Farcau C, Astilean S. Mapping the SERS efficiency and hot-spots localization on gold film over nanospheres substrates. *J Phys Chem C*, 2010, 114: 11717–11722

55 Yang SC, Yang DJ, Kim J, Hong JM, Kim HG, Kim ID, Lee H. Hollow TiO_2 hemispheres obtained by colloidal templating for application in dye-sensitized solar cells. *Adv Mater*, 2008, 20: 1059–1064

56 Romanov SG, Korovin AV, Regensburger A, Peschel U. Hybrid colloidal plasmonic-photonic crystals. *Adv Mater*, 2011, 23: 2515–2533

57 Ding B, Hrelescu C, Arnold N, Isic G, Klar TA. Spectral and directional reshaping of fluorescence in large area self-assembled plasmonic-photonic crystals. *Nano Lett*, 2013: 13, 378–386

58 Xiong Y, Tang Z. Role of self-assembly in construction of inorganic nanostructural materials. *Sci China Chem*, 2012, 55: 2272–2282

59 Hu S, Wang X. From cluster assembly to ultrathin nanocrystals and complex nanostructures. *Sci China Chem*, 2012, 55: 2257–2271

60 Liu JW, Liang HW, Yu SH. Macroscopic-scale assembled nanowire thin films and their functionalities. *Chem Rev*, 2012, 112: 4770–4799